ISSN: 2538-5887; Pathobiology Research. 2022;25(4): 23-29

Topological Causal Analysis Reveals Two Stages of In Vitro neural Network Maturation: Network Expansion and Network Reinforcement

ARTICLE INFO

Article Type
Original Research

Authors

Zahra Naghdabadi[1]

Sara Mirsadeghi[2,3]

Sahar Kiani[2,3,4*]

1Department of Electrical Engineering, Sharif University of Technology, Tehran 1458889694, Iran.
2Department of Stem Cell and Developmental Biology, Cell Science Research Center, ROYAN Institute for Stem Cell Biology and Technology, ACECR, Tehran, Iran.
3Department of Brain and Cognitive Sciences, Cell Science Research Center, ROYAN Institute for Stem Cell Biology and Technology, ACECR, Tehran, Iran.
4Center for Cognitive Science, Institute for Convergence Science & Technology, Sharif University of Technology, Tehran 14588-89694, Iran.

***Corresponding author:**

Sahar Kiani
sahar_kiani@royaninstitute.org
skiani2536@gmail.com
sahar.kiani36@sharif.edu

ABSTRACT

Background: Topological data analysis (TDA) in neural networks and its advantages over traditional methods by capturing higher-order relationships and complex structures within the network is examined in this research. TDA provides insights into cognitive processes by analyzing multi-scale interactions among neural activities and is increasingly utilized in both brain science and psychological research.

Methods: The methodology explores neural data from multi-electrode array (MEA) recordings of rat cortical cells to study neural ensemble behaviors and connectivity. Additionally, it critiques existing methods like Granger causality analysis (GCA) for their limitations in interpreting neural data.

Results: According to our findings, the number of spiking activities and the number of active MEA electrodes rise from the 10th to the 60th day in vitro (DIV). Burst activities peaked between 30 and 50 DIV, while the firing rate in active electrodes continued to increase until 30 DIV. Furthermore, the average burst length exhibited a consistent rise until 50 DIV. However, the percentage of spikes involved in burst activities displayed a non-monotonic pattern, initially declining until 30 DIV and rising again in subsequent days. Topological measures of causal relations during development showed network expansion in early days and reinforcement of the established connections in the subsequent days.

Conclusion: In summary, TDA provides qualitative insights into network status based on quantitative metrics and established thresholds. Using TDA on MEA cell cultures, we were able to distinguish two stages of network development. While we focused on primary neuronal cells derived from rat cortices, MEA technology is versatile enough to monitor the developmental stages of any neuronal type, including those derived from human sources. Applying topological causal analysis on developing neural networks sheds light on the process of network initiation, maturation, and stabilization.

Keyword: topological data analysis (TDA), neural network, multielectrode array (MEA)

Copyright© 2020, TMU Press. This open-access article is published under the terms of the Creative Commons Attribution-NonCommercial 4.0 International License which permits Share (copy and redistribute the material in any medium or format) and Adapt (remix, transform, and build upon the material) under the Attribution-NonCommercial terms

INTRODUCTION

The application of topological data analysis (TDA) in network neuroscience offers novel ways to understand brain anatomy, function, and organization (1). In contrast to traditional methods like graph theory, which focus on pairwise interactions, TDA excels at capturing higher-order relationships and complex structures that occur across multiple scales in the brain (2). Topology itself describes relationships at macro, meso, and micro scales, encompassing gene regulatory networks, protein interactions, neural signaling patterns, and brain-environment dynamics (3-4). By analyzing these multi-scale interactions, TDA provides deeper insights into both spontaneous and task-evoked neural activities, as well as their links to cognitive processes and behavior. As a result, TDA is

increasingly recognized as an efficient tool in both brain and psychological sciences. It reveals how the unique topology of individual neural networks underlies the diversity of human intellectual abilities (5).

In addition, TDA is a promising framework for addressing key open questions in neuroscience, such as how neural codes are shaped by external stimuli and how neural populations contribute to larger network behavior (6). TDA can process a variety of neural data types collected through diverse techniques. For example, it has helped explain spatial memory encoding in the brain of a moving rat (7) and, when integrated with fMRI, has distinguished healthy states from pathological conditions in neurodevelopmental and neurodegenerative diseases (8). Another widely used tool is the multi-electrode array (MEA), a non-invasive technology for long-term neural recordings (9-10). MEAs are essential in academic research for spike and burst detection (11), studying connectivity in developing neurons (12), and modeling neural networks (13). Importantly, MEAs provide insights into neural ensemble behavior without the complexities of in vivo conditions, making them a valuable tool for causality analysis. (14-15).

Causal relationships in mature neural networks are often studied using Granger causality analysis (GCA) (16), a method originally developed in economics. However, GCA has several limitations in neuroscience. It requires statistical knowledge to interpret the weight matrix outputs, focuses only on highly repeated patterns, and does not adequately account for the biological context of neural data (17). These issues can lead to biased or misleading results, making it difficult to fully understand neural interactions. Therefore, there is a need for a more biologically grounded approach.

To address these limitations, we propose a new methodology: Topological Causal Analysis (TCA). TCA builds on TDA principles to identify causal relationships between neurons in a way that is both physiologically meaningful and easy to interpret. We believe that the spike data, including event timing and electrode information, is a sufficient resource for causality analysis. Our approach focuses on simple action potential propagation rules and treats causal graphs as topological objects, allowing for clear and intuitive interpretations. By combining the strengths of TDA with causal analysis, we aim to offer a more robust and accessible framework for understanding neural network dynamics. This approach not only provides a fresh perspective on neural interactions but also has potential implications for broader fields such as artificial intelligence and computational neuroscience.

MATERIALS AND METHOD

Neural cell isolation and culture on MEA. Neural and glial cells were cultured on multi-electrode arrays (MEA) from rat cerebral cortex tissue isolated between embryonic days 16-18. The isolation procedure followed a previously established protocol with some modifications (18). Briefly, a pregnant rat was euthanized in accordance with institutional guidelines. The abdominal skin and peritoneum were cut to expose the abdominal cavity, and the uterus containing the embryos was transferred to an ice-cold dissection buffer composed of Hank's Balanced Salt Solution (HBSS, 14025-050; Gibco), 20 mM glucose (G7021; Sigma), 1% GlutaMAX (35050-038; Gibco), 100 U/ml penicillin-streptomycin, and 50 mg/ml gentamycin (15750-060; Gibco). Each embryo was decapitated using sharp scissors, and the head skin and skull tissue were carefully removed with micro scissors to expose the cortical lobes. The superficial cortical layer was isolated from the brain using small curved forceps and placed in phosphate-buffered saline (PBS-, 10010-031; Gibco) with 20 mM glucose, 1% GlutaMAX, 100 U/ml penicillin-streptomycin, and 50 mg/ml gentamycin. The meninges were carefully removed to prevent contamination by blood cells, and the cortical tissue was dissected into small pieces. Neuronal cells were then isolated from the tissue using enzymatic digestion with 0.25% Trypsin-EDTA (15400-054; Gibco) for 20 minutes at 37°C.

Before cell seeding, sterile multi-electrode arrays (60MEA200/10iR-ITO; Multichannel Systems) were coated with Poly-L-ornithine (PLO, P4957; Sigma) for one hour, followed by

Laminin (L2020; Sigma) for three hours at 37°C. The isolated neurons were cultured in Neurobasal™ Medium (21103-049; Gibco) supplemented with 2% B27 (17504-044; Gibco), 1% horse serum (H1138; Sigma), 1% GlutaMAX (35050-038; Gibco), 100 U/ml penicillin-streptomycin, 33 mM glucose (G7021; Sigma), and 0.04% W/V sodium bicarbonate (S5761; Sigma). The medium was fully replaced 24 hours after seeding, and then partially changed (half-medium replacement) every other day.

Multi-electrode array recording and data acquisition. All electrophysiological recordings were carried out inside a humid (i.e., 95% R.H.) incubator at 37°C and 5% CO2. To prevent media evaporation and optimize recording conditions, each MEA was sealed with fluorinated Teflon thin film (MEA-MEM-set5, Multichannel systems, Harvard Bioscience) that selectively allows gas permeability but blocks water evaporation and microorganism contamination. We recorded spontaneous activity of the neurons. Raw electrical potentials, detected extracellularly from each microelectrode, were amplified using an electronic amplifier (MEA1060, Multichannel systems, Harvard Bioscience), sampled at 25 kHz/electrode, and digitized at 16 bits resolution. The recorded extracellular potential traces were stored on disk via software (MC-Rack, Multichannel systems, Harvard Bioscience) for subsequent offline analyses.

Data analysis criteria. In this study, data analysis was conducted in several stages. Raw data was prepared using custom code in MATLAB 2014Ra and C#. Spikes were detected by applying an amplitude threshold to the filtered data, which was processed using a 4th-order Butterworth band-pass filter with a frequency range of 300-5000 Hz. The subsequent analysis focused on key spike characteristics, including the number of active electrodes, spike timing, and spike shape. The analysis was divided into four categories: (1) spike analysis, (2) burst analysis, (3) causality analysis of bursts, and (4) relative analysis between these groups. In this section, we explicitly define all the metrics used and provide a rationale for their selection. Our causality analysis is straightforward, focusing on causal graphs as geometric or topological objects, making it easy to interpret without requiring statistical expertise. The dataset includes 65 recordings from 7 plates (59 electrodes), each lasting 15 minutes, collected over more than 50 days in vitro (DIV).

(1) Spikes statistical analysis

Statistical analysis in this context refers to tracking changes in metrics over time to assess how a small neural network on an MEA evolves during maturation. As neurons develop, significant changes are expected in the number of spikes, bursts, active electrodes, and the connectivity between electrodes. By measuring these factors over a defined time period in vitro, we can evaluate the level of neuronal maturity and identify various stages of the maturation process.

Number of spikes. The number of spikes is defined as the count of local maxima exceeding 5.2* standard deviation, with a temporal gap of more than 2 milliseconds between them. This metric is a fundamental measure in each recording, representing the activity level of individual cells in the network.

Number of active electrodes. The number of active electrodes indicates the expansion of the neural ensemble as it develops in vitro. As neurons grow and interact, the network is expected to become more complex over time. The count of active electrodes provides insight into the network's overall scale. In this study, electrodes that detect high-frequency events (above 300 Hz), whether individual spikes or bursts, are classified as active electrodes.

Spike firing rate (SFR). Changes in spike count and the number of active electrodes during the in vitro development of the network occur independently. However, the ratio of these changes at each stage of development is also important. This ratio is captured by the relative firing rate, defined as follows:

$$Spike\ Firirng\ Rate\ (SFR) = \frac{\#spike}{\#active\ channels \times time\ in\ min}$$

Subsequently, the Burst Firing Rate (BFR) is defined in a similar manner.

Average spike amplitude in the recording. Spike amplitude is the peak-to-peak voltage of each detected spike. First, the average spike amplitude is calculated for each electrode, and then a weighted average is computed across all electrode.

$$avg\ spike\ amp.in\ rec. = \frac{\sum(avg\ spike\ amp.\ \times\ \#spikes)}{\sum \#\ spikes}$$

where the sum is taken over all electrodes, with the summands calculated for each individual electrode.

(2) Bursts statistical analysis.

Neuronal bursts are interpreted as codes of communication between neurons (19). In this context, a burst refers to a sequence of spikes occurring in a single electrode, with an inter-spike interval of less than 10 milliseconds.

Number of bursts. The number of bursts is defined as the count of spike chains with inter-spike intervals of less than 10 milliseconds. This metric serves as an indicator of the amount of communication occurring within the network during a 15-minute MEA recording.

Burst firing rate (BFR). As explained in the SFR section, we define the Burst Firing Rate (BFR) as follows to assess the different stages of network maturation:

$$Burst\ Firirng\ Rate\ (BFR) = \frac{\#burst}{\#active\ channels \times time\ in\ min}$$

Percentage of spikes in a burst, is defined as follows:

$$Percent\ of\ spikes\ in\ a\ burst = \frac{\#spike}{\#burst}.$$

This metric also reflects the various stages of network maturation.

Average number of spikes in burst (burst length). To assess the length of bursts, we calculated the average number of spikes per burst. In our study, burst lengths varied from 2 to 17 spikes.

(3) Bursts topological causality analysis.

It has been reported that following voltage stimulation (biphasic rectangular voltage pulses with amplitudes ranging from 100 to 900 mV and pulse widths of 400 µsec), an immediate response can be detected in the surrounding electrodes. This response consists of three phases: (1) a direct response with latencies between 3 and 10 msec, (2) a postsynaptic response with latencies of 5 to 50 msec, and (3) a burst response occurring within a range of 50 to 200 msec (20). Accordingly, we established a latency of 100 msec among firing neurons as a reliable measure of signal propagation in intact networks. Thus, two bursts are considered causal if the temporal distance between them is less than 100 msec. A sequence of bursts with inter-burst intervals of less than 100 msec is referred to as a causal chain or causal relationship.

Number of causal relations. This indicates the number of causal chains (neuronal conversations) that begin with a burst and are followed by additional bursts within 100 milliseconds. A chain terminates when no burst is detected within 100 milliseconds of the last burst.

Pattern of causal relations. This qualitative indicator reflects the spatial expansion of the network and is represented in the activity figures from the MEA. The pattern may vary for each neural network on the MEA and is expected to follow an autonomous trajectory in neural networks derived from different regions of the brain. (21).

In the remaining metrics, we analyze causal graphs as topological objects and track the causal status of networks using these metrics. This perspective has emerged recently in neuroscience (1,22). We adopt a similar viewpoint to develop Topological Causality Analysis (TCA).

Connectivity of causal network. The causal network is represented as a graph, with electrodes as vertices. electrode A and electrode B are connected by an edge if there exists a causal chain in which electrode B produces a burst following a burst from electrode A. We employ various concepts from graph theory to explore these graphs in greater depth.

Network size (Number of involved electrodes). To assess the growth of the network, we consider the number of electrodes involved in causal relations. By treating the network as a graph, we define the network size as the number of vertices.

Network causal strength. It is widely accepted that causality is much stronger in an interwoven network than in a sparse network. Therefore, we use the Average Vertex Degree (AVD) of this graph as a metric to indicate network strength. The degree of a vertex v, denoted as d(v), is defined as the number of edges emanating from that vertex. Hence, the AVD metric is calculated as

$$AVD := \frac{\sum d(v)}{\#vertices\ of\ G} = \frac{2 \times \#Edges\ of\ G}{\#vertices\ of\ G},$$

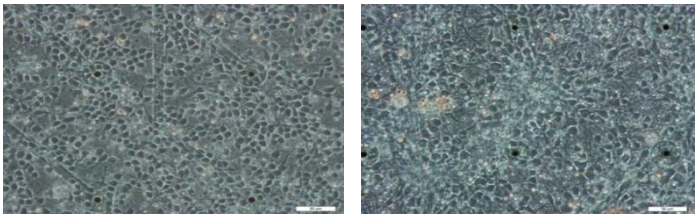
where G is the causality graph and the summation is taken over all vertices of G. The second equality states that the sum of the degrees of a graph is equal to twice the number of edges, which is straightforward to prove. (23-24).

RESULTS

In this study, we cultured neural cells in a simple medium and applied straightforward definitions derived from previous in vitro closed-loop experiments on neural networks to demonstrate causal relationships. It has been reported that following voltage stimulation in a multi-electrode setting, an immediate response can be detected in the surrounding electrodes. This response consists of three phases: an early direct response, a postsynaptic response, and a late burst response (20). Accordingly, we considered topological structure of causal relations based on chain of burst activities and studied how measures of network topology change during cell maturation. Details of metrics definition and measurements are explained in the materials and methods section.

Isolated neural cells emerged a long-term survival and spiking activity on MEA.

The neural cells were cultured in a simple medium combination, and their morphological changes were monitored via light microscopy twice a week. The cells began to extend their dendrites and axons 24 hours after seeding (Figure 1a) and became increasingly interconnected during in vitro development (Figure 1b). Several cultures exhibited spiking activity starting at 8 days in vitro (DIV), while the majority demonstrated synchronous activity from 15 DIV and continued to thrive until 40 to 60 DIV.



In addition to morphological changes, the electrical activity of the neural cells was recorded three times a week. During the maturation process, spiking activity increased significantly from zero to 30,000 spikes in the first 30 days in vitro (DIV) and stabilized in the following 10 days (Figure 2a). The number of bursts increased to over 3,500 during the period from 30 to 45 DIV (Figure 2b). On average, each active electrode fired more than 25 spikes per minute during this timeframe, indicating that the spike firing rate increased by more than 50% in the first month of maturation (Figure 2c). Additionally, the average burst length increased by 50%, exceeding 4.5 spikes by 40 DIV (Figure 2d).

Figure 1 shows the light microscopy view of cultured neural network**. (a)** In the first DIV, neural cells' soma adheres to the protein coated surface of the MEA. **(b)** Neural cells are able to extend their dendrites and axons to shape a recondite network on MEA, over time.

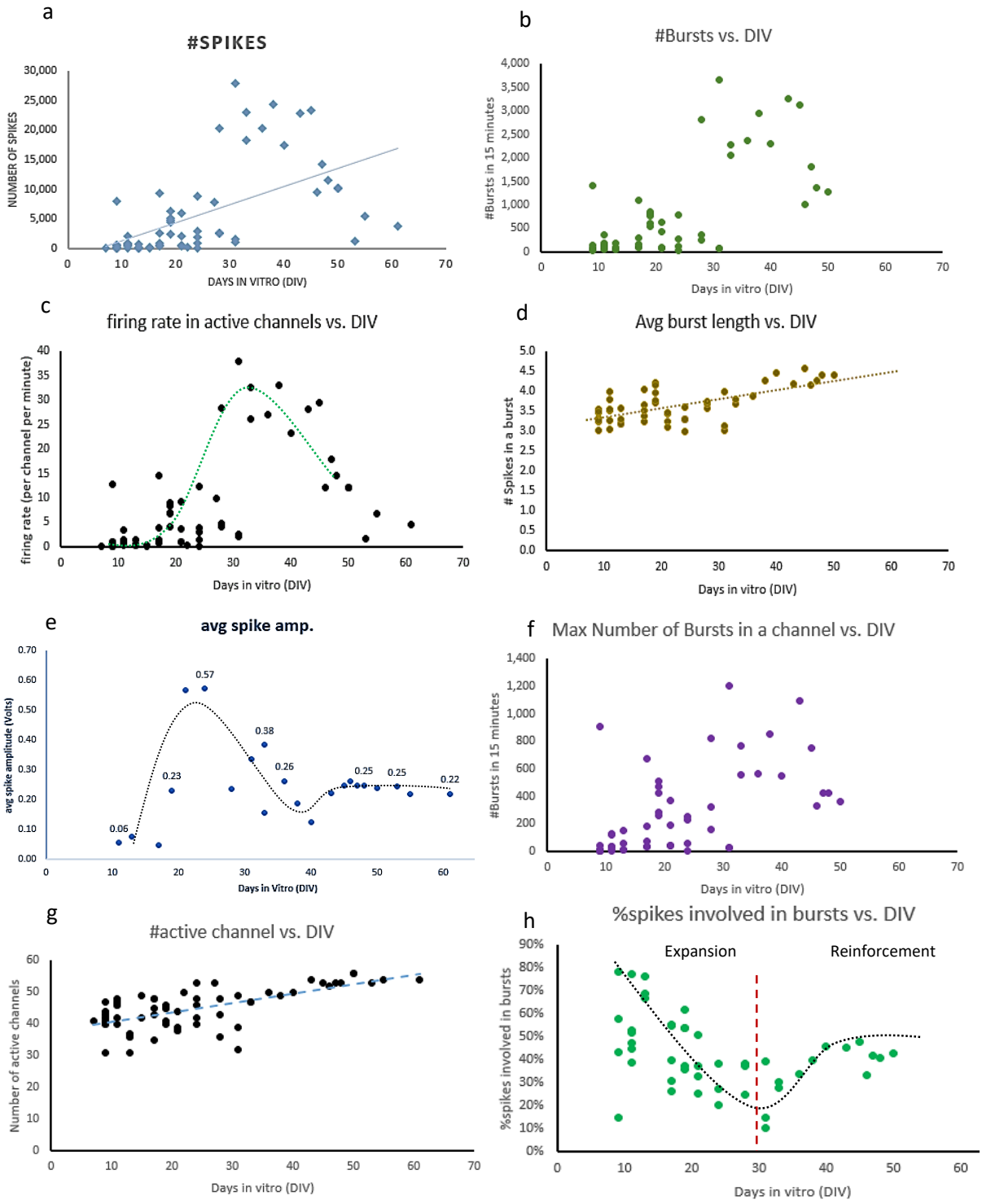


Figure 2. Isolated neural cells emerged a long-term survival on MEA. Number of spikes **(a)** and bursts **(b)** in a recording session increase during maturation. **(c)** Spike firing rate rises to 40 spikes/min per electrode in 30 DIV and remains more than 20 spike/min during 30-45 DIV. **(d)** The average burst consists of more spikes as time goes on. Average burst length starts from 3.5 in early DIV and increases steadily to 4.5 after 45 DIV. **(e)** Average amplitude of spikes in a single plate first increases and after reaching a climax of 570 millivolts in 21 DIV, approaches 220 millivolts. **(f)** Maximum number of bursts observed in electrodes increased after 30 DIV and is more than 600 bursts during the next 15 days. **(g)** Number of active electrodes increased so that after 45 DIV more than 50 of 59 electrodes are active. **(h)** Percentage of spikes involved in bursts decreases from 80% in 9 DIV to 10% in 30 DIV, increases during the next 15 days, and stabilizes at 50%.

Analysis of the cortical neuron recordings revealed significant variations in spike amplitude across different DIVs. In the early days, spike amplitude increased, reaching a peak of 570 millivolts on 21 DIV before declining. After 45 DIV, spike amplitude stabilized at around 250 millivolts (Figure 2e). The maximum number of bursts observed in an electrode during a 15-minute recording increased dramatically from 200 bursts at 17 DIV to 1,200 bursts at 30 DIV, remaining above 550 bursts during 30 to 45 DIV (Figure 2f).

The number of active electrodes also increased by 50% throughout cell maturation. By 2 months, spiking was detectable in an average of 55 electrodes, indicating that 93% of the neurons in the network were capable of producing spikes (Figure 2g). The percentage of spikes involved in burst activities decreased from 80% at 10 DIV to 10% at 30 DIV. However, during the period from 30 to 45 DIV, this percentage increased to 50% and stabilized at that level (Figure 2h).

More neurons participate in causal relations as neural cells develop in vitro.

Causal relations are represented as a graph, with MEA channels (electrodes) as vertices. Two electrodes are connected if there exists a causal chain of bursts between them. During in vitro development, the size of the neural network—measured by the number of electrodes involved in causal relations—expanded significantly (Figure 4a). By 50 days in vitro (DIV), the number of electrodes in causal relations increased to 25, with over 40% of the microelectrode array (MEA) area engaged in these interactions. The total number of causal relations indicated by graph edges also increased during development (Figure 4b). Over time, the number of causal chains increased exponentially, contributing to a stronger and more reliable network (Figure 5a). Simultaneously, the average vertex degree (AVD) in the causal graphs increased; for instance, the AVD was less than 2 at 20 DIV, while it exceeded 8 after 40 DIV (Figure 4c). Additionally, burst durations lengthened, with the average burst length increasing from 3 to 4.5 spikes per burst (Figure 2d).

Neural network maturation in vitro has two stages: Network Expansion and Network Reinforcement

After 30 DIV, more than 200 causal relations were observed, indicating that the network was entering a new stage of development (Figure 5a). Between 30 and 45 DIV, the number of causal electrodes (network pattern) remained stable (Figures 4a), while the connections between these MEA channels (electrodes) strengthened significantly; the number of edges in the causal graphs increased from 12 at 25 DIV to 80 at 46 DIV (Figure 4b). The spatial pattern of causal relations during maturation illustrates that causal relations expand and involve more electrodes in the first 30 days (Figure 3a). Then, from 30 to 45 DIV, relations in the stablished neural network are reinforced and optimized as captured by the average vertex degree (Figure 3b, 4c). We observed that the center of activity also shifts during the first 30 days, coinciding with the network's expansion suggesting that certain regions of the network were more likely to participate in causal relations than others (Figure 3). Hence, the two phases of neural networks maturation vary in topological metrics of causal relations.

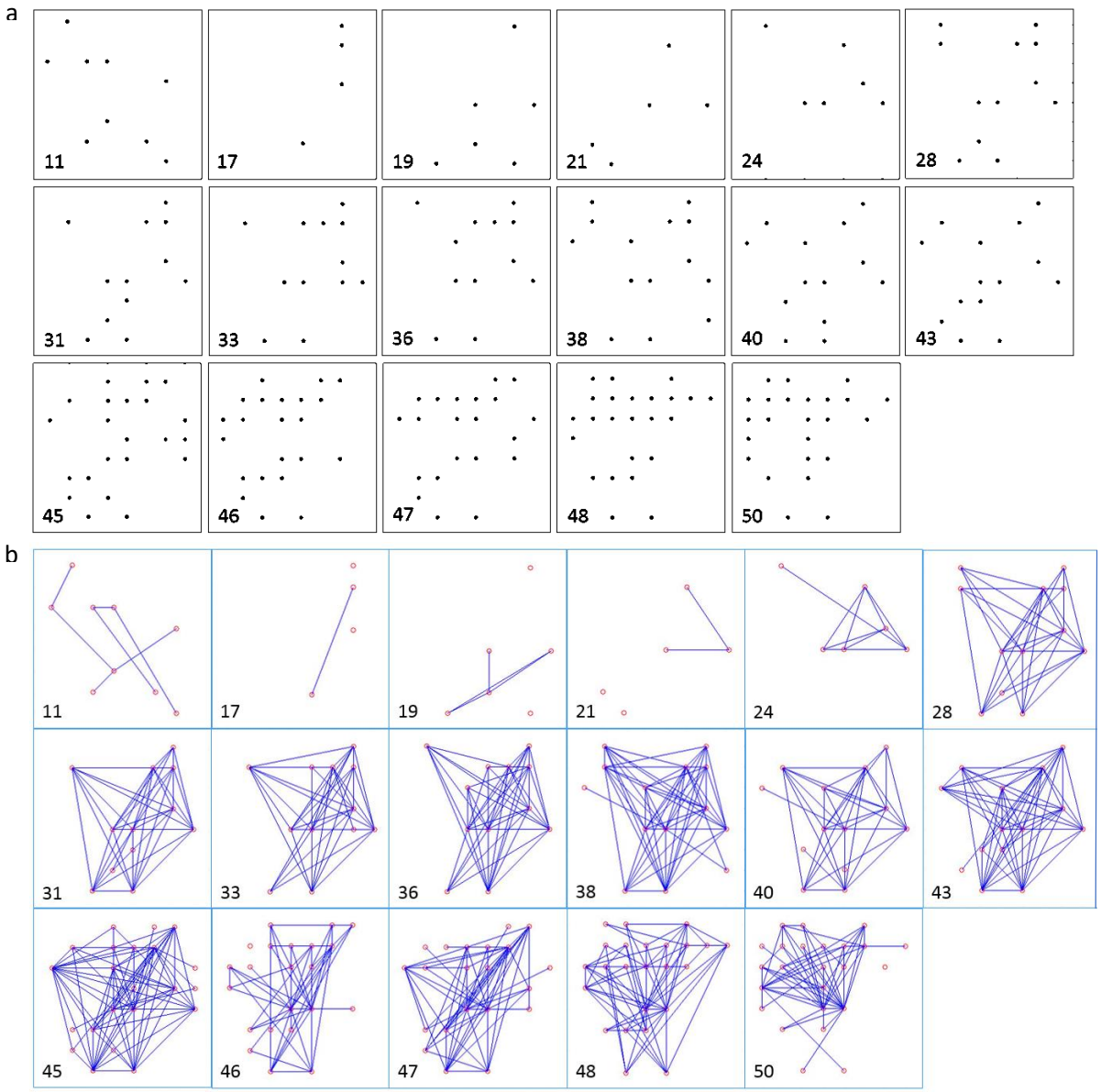


Figure 3. Topological Causality Analysis (TCA) plots for an example MEA plate. **(a)** Active electrodes in causal relations in an MEA plate. The numbers in each box illustrate DIV. Each box shows the MEA plate and points illustrate electrodes active in causal burst chains. During culture maturation, the network expands and new electrodes are involved in the network. **(b)** Causal relations in a single plate during culture maturation. Each box shows the MEA plate where the red points (vertices) are involved electrodes and blue edges connect electrodes in order of appearance in causal burst chains. Over time, the network expands in area and gets dense. After 45 DIV, the network undergoes attenuation. Only the stable parts of the network remain in causal relation.

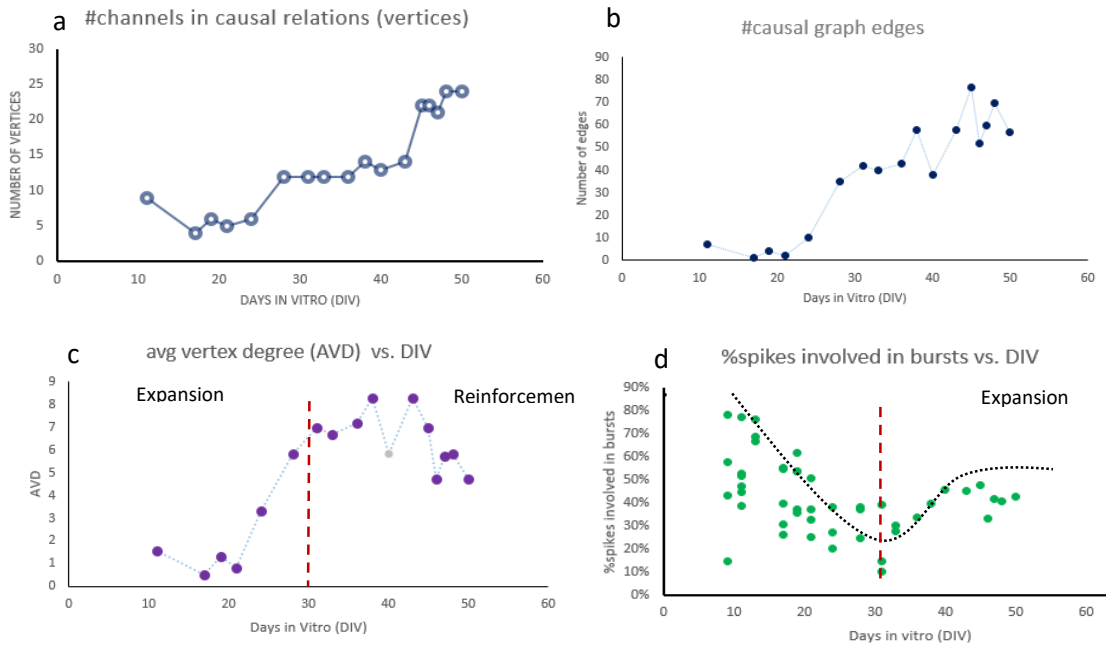


Figure 4. Topological Causality Analysis (TCA); **(a)** Network size expands during time as the number of electrodes involved in causal relations increase significantly from 10 to 25. **(b)** Also, the network becomes stronger since the number of edges exceeds to 80 **(c)** The average vertex degree (AVD) is about 1 during early DIV and exceeds to 8 after 35 DIV. Hence, the network becomes more interwoven. **(d)** While in early days, most activities occur in bursts rather than single spikes, as time goes on, more cells become active and make single spikes but these spikes are not in autonomy. Thus, the percentage of spikes in a burst decrease significantly during 10-30 DIV. This is the first stage of network maturation. In the second stage, during 30-40 DIV, the network flourishes, and this percentage rises to reach an asymptote of 50%. Since the maturation pattern of MEA plates are not all the same, figure (a), (b), and (c) are platted for an example MEA plate.

The Causality-Burst Regression Model (CBRM) takes the number of bursts as input and predicts the number of causal communications in the network, irrespective of the culture's age. This model is derived from a regression analysis of experimental data and is expressed as follows.

Causality-Burst Regression Model (CBRM): Let x be the number of bursts. Then, the number of given causal relationship is given by:

$$\#causal\ relations\ = \max\{0.1153\ x - 24.616, 0\}$$

It is important to note that if the number of bursts is less than 214 (the threshold), this model does not predict the existence of any causal relations in the network. This underscores the fact that during the initial stage of network development, causal relations are not formed. The value 214 corresponds to the x-intercept, where the line intersects the x-axis in the CBRM.

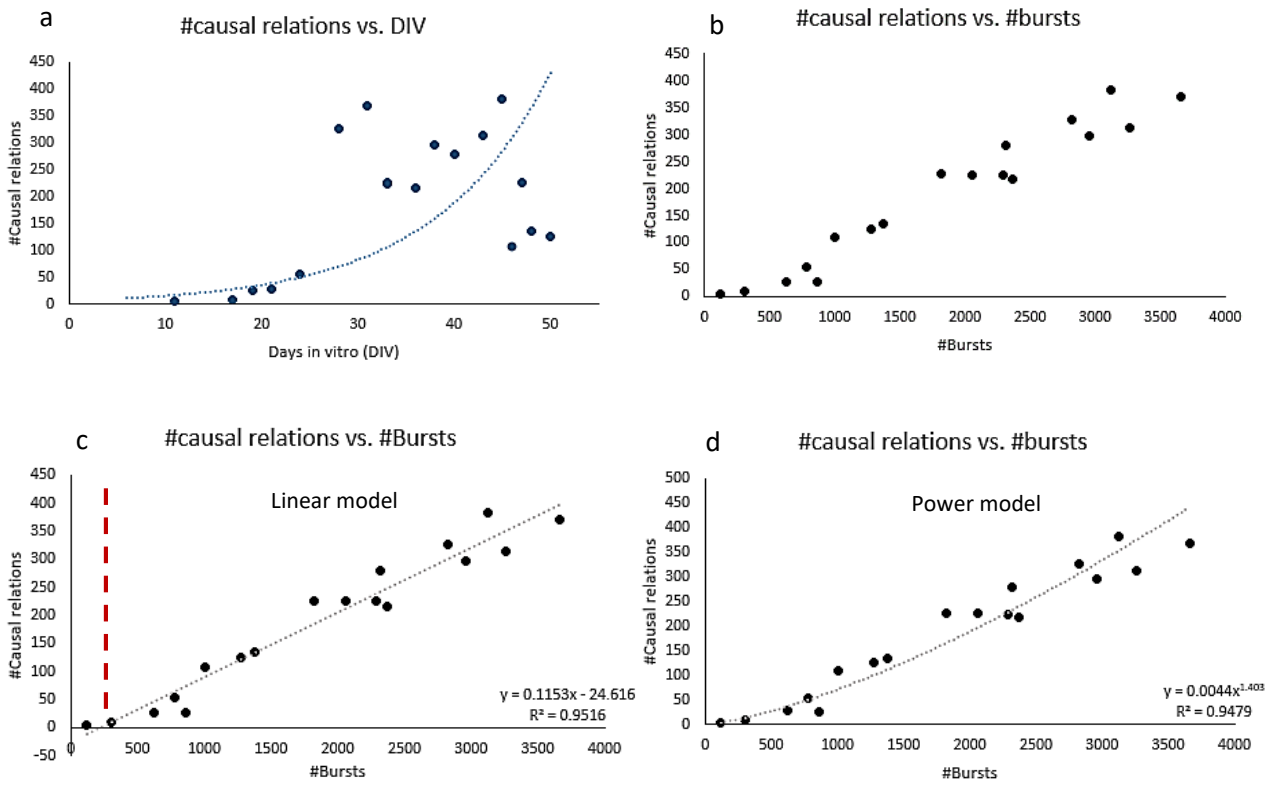


Figure 5. Causality – Burst Regression Model (CBRM). **(a)** Number of causal relations increases exponentially and exceeds 200 relations in 15 minutes after 30 DIV. **(b)** Number of causal relations has direct relationship with number of bursts. **(c)** Here we fit the data to a linear model of form y = ax + b and **(d)** a power model of y = axb. In both models, R2 is more than 94%. The power model has an exponent of 1.4 together with a small coefficient. Hence, the relationship is linear and the equation model is y = 0.115x – 24.616. Moreover, there exists a threshold on the number of bursts below which no causal relation is expected.

Discussion

In this study, we proposed a physiologically relevant method to investigate causal relationships among in vitro developing neurons, utilizing Topological Causality Analysis (TCA) principles. This approach treats causal graphs as topological objects and defines metrics that reflect widely accepted concepts of synaptic causality, such as the propagation period of action potentials between connected neurons. Previous studies have demonstrated that evoked responses due to stimulation can be transferred through immediate synapses within approximately 200 milliseconds (20,25) lending credence to our methodology.

According to our findings, the number of spiking activities and active electrodes rise from the 10th to the 60th day in vitro (DIV) (Figures 3a and g). Burst activities peaked between 30 and 50 DIV, while the firing rate in active electrodes continued to increase until 30 DIV. Furthermore, the average burst length exhibited a consistent rise until 50 DIV (Figures 3b-f). However, the percentage of spikes involved in burst activities displayed a non-monotonic pattern, initially declining until 30 DIV and rising again in subsequent days (Figure 4d). The fluctuations in average spike amplitudes (Figure 2e) can be attributed to factors such as the distance between neurons and electrodes, as well as the ongoing neuronal plasticity and migration. Consistent with prior reports, all calculated indices indicate that the characteristics of cultured cells evolve towards greater maturity and complexity over the 60 DIV period (26).

Upon closer examination, the percentage of spikes in bursts decreases during the first month before increasing and stabilizing at approximately 50%. This observation underscores the distinct phases of development within the network. In the initial stage, neurons generate individual spikes and stabilize independently. In contrast, the second stage is characterized by more frequent communication among stabilized cells, leading to increased involvement of spikes in bursts. Therefore, we designate the first 30 days of network development as the **expansion stage** and the subsequent days as the **reinforcement stage**. These developmental stages are reflected in metrics such as the maximum quantity of bursts per electrodes (Figure 2f), the number of causal relations (Figure 5a), and the number of vertices (Figure 4a) and edges in the causal graph (Figure 4b), as well as the average vertex degree (AVD) of the causal graph (Figure 4c). Notably, the AVD provides a more robust and informative measure compared to traditional functional connectivity metrics averaged over electrodes.

During the expansion stage, the network expands its branches and establishes more connections between neurons, a phenomenon that is also visible through light microscopy (Figure 1). In the reinforcement stage, the network becomes more advanced and complex. Our use of TCA reveals that the number of edges in causal graphs increases significantly compared to the expansion stage, suggesting that neural cells develop a more sophisticated mode of communication. In this context, individual spikes can be seen as letters, while bursts (or spike trains) represent intricate sentences that facilitate complex interactions among neurons after 30 DIV.

Concurrent with our findings, previous research employing non-linear Granger causality analysis has been used to identify functional maps of various network sizes, including small-scale ensembles on microelectrode arrays (27). However, to the best of our knowledge, the two distinct stages of network maturation have not been delineated on MEAs using Granger causality methods. Our study introduces new metrics and concepts, such as the average vertex degree (AVD) and the number of causal MEA channels (electrodes), to the existing literature on neural network maturation.

Additionally, we introduced a linear Causality-Burst Regression Model (CBRM), which illustrates the causal status of a network based on instantaneous burst frequency measurements. This model confirms the existence of a threshold in the number of bursts that correlates with neuronal causality. According to the CBRM, meaningful causal neural coding is expected only when the overall burst count exceeds this threshold. The CBRM establishes an explicit relationship between statistical metrics and the causality status of the network. While causality analysis can be complex and time-consuming, the statistical metrics used in CBRM are straightforward to measure. Consequently, CBRM offers a simple and robust method to determine the development of causal relations within a network by merely counting bursts over a 15-minute interval. This approach can facilitate predictions about the impact of various manipulations on neural connectivity during in vitro development, including traditional assessments of drug effects (28) or stimulus (29) on network, specifically on its causality. We also speculate that different neuronal types isolated from various brain regions, or even from different species, could each possess distinct CBRM models. Moreover, we conjecture that all such models may exhibit linear characteristics or approach a linear asymptote over time in vitro. In our study of rat cortical neurons, the CBRM was found to be linear, with a leading coefficient of 0.1153 and a y-intercept of -24.616.

TCA is a novel approach that can be applied to other scientific fields, as it was developed specifically for biological signals without requiring extensive knowledge of mathematics or statistics. This study represents the first application of TCA in such a context. TCA shifts the perspective on neural networks from viewing them as mere time series generators to considering them as graphs (topological objects). This methodology allows for comparisons between network size and connectivity while identifying stable patterns in mature networks. In summary, TCA provides qualitative insights into network status based on quantitative metrics and

established thresholds. While we focused on primary neuronal cells derived from rat cortices, MEA technology is versatile enough to monitor the developmental stages of any neuronal type, including those derived from human sources (30). Furthermore, this technique can be employed in organotypic slice recordings, enabling the characterization of a diverse range of neuronal networks (31). TCA, when coupled with functional MRI, has been utilized to explore network transformations across the entire brain, including the frontal lobe in attention-deficit hyperactivity disorder (ADHD) (32). The growing interest in developing in vitro disease models for neurodegenerative disorders has become a focal point among developmental biologists (33). Therefore, we propose that integrating MEA technology with stem cell methodologies and TCA will advance neuroscience to a higher level of in vitro assessments of the human brain (brain-on-chip) in a multidisciplinary context.

ACKNOWLEDGEMENT

Our sincere thanks go to the ROYAN institute for financial support.

FUNDING

The present research was funded by the ROYAN Institute, Department of Brain and Cognitive Sciences.

DISCLOSURE

All authors declare no conflict of interest.

AUTHOR CONTRIBUTIONS

Zahra Naghdabadi analyzed data and innovated the formula and mathematics model, Sara Mirsadeghi cultured the neural cells and recording data by MEA, Sahar Kiani supervised the whole project, discovered the grant sources. All authors contributed to writing the manuscript.

REFERENCES

[1] Bullmore, E. and Sporns, O. (2009) 'Complex brain networks: Graph theoretical analysis of structural and functional systems', *Nature Reviews Neuroscience*, 10(3), pp. 186–198. doi: 10.1038/nrn2575.

[2] Expert, P. *et al.* (2019) 'Editorial: Topological neuroscience', *Network Neuroscience*, 3(3), pp. 653–655. doi: 10.1162/netn_e_00096.

[3] Carlsson, G. (2009) *Topology and data*, *Bulletin of the American Mathematical Society*. doi: 10.1090/S0273-0979-09-01249-X.

[4] Freeman (2018) 'Network neuroscience', *Physiology & behavior*, 176(1), pp. 139–148. doi: 10.1117/12.2549369.Hyperspectral.

[5] Barbey, A. K. (2018) 'Network Neuroscience Theory of Human Intelligence', *Trends in Cognitive Sciences*. Elsevier Ltd, 22(1), pp. 8–20. doi: 10.1016/j.tics.2017.10.001.

[6] Curto, C. (2017) 'What can topology tell us about the neural code?', *Bulletin of the American Mathematical Society*, 54(1), pp. 63–78. Available at: http://dx.doi.org/10.1090/bull/1554.

[7] Dabaghian, Y. *et al.* (2012) 'A Topological Paradigm for Hippocampal Spatial Map Formation Using Persistent Homology', *PLoS Computational Biology*, 8(8). doi: 10.1371/journal.pcbi.1002581.

[8] Lee, H. *et al.* (2017) 'Integrated multimodal network approach to PET and MRI based on multidimensional persistent homology', *Human Brain Mapping*, 38(3), pp. 1387–1402. doi: 10.1002/hbm.23461.

[9] Wheeler, B. C., Nam, Y. and Wheeler, B. C. (2011) 'In vitro microelectrode array technology and neural recordings.', *Critical Reviews™ in Biomedical Engineering*, 39(1), pp. 45–61. doi: 10.1615/CritRevBiomedEng.v39.i1.40.

[10] Spira, M. E. and Hai, A. (2013) 'Multi-electrode array technologies for neuroscience and cardiology', *Nature Nanotechnology*. Nature Publishing Group, 8(2), pp. 83–94. doi: 10.1038/nnano.2012.265.

[11] Opitz, T., De Lima, A. D. and Voigt, T. (2002) 'Spontaneous development of synchronous oscillatory activity during maturation of cortical networks in vitro', *Journal of Neurophysiology*, 88(5), pp. 2196–2206. doi: 10.1152/jn.00316.2002.

[12] Lonardoni, D. *et al.* (2017) 'Recurrently connected and localized neuronal communities

initiate coordinated spontaneous activity in neuronal networks', *PLoS Computational Biology*, 13(7), pp. 1–27. doi: 10.1371/journal.pcbi.1005672.

[13] Valenza, G. *et al.* (2016) 'Stochastic modeling of spontaneous bursting activity to simulate neural responses of in-vitro networks on multielectrode arrays', *Proceedings of the Annual International Conference of the IEEE Engineering in Medicine and Biology Society, EMBS*, 2016-Octob, pp. 1616–1619. doi: 10.1109/EMBC.2016.7591022.

[14] Granger, C. W. J. (2008) 'Investigating Causal Relations by Econometric Models and Cross-Spectral Methods', in *Essays in Econometrics vol II: Collected Papers of Clive W. J. Granger*, pp. 31–47. doi: 10.1017/ccol052179207x.002.

[15] Seth, A. K., Barrett, A. B. and Barnett, L. (2015) 'Granger causality analysis in neuroscience and neuroimaging', *Journal of Neuroscience*, 35(8), pp. 3293–3297. doi: 10.1523/JNEUROSCI.4399-14.2015.

[16] Cadotte, A. J. *et al.* (2008) 'Causal measures of structure and plasticity in simulated and living neural networks', *PLoS ONE*, 3(10). doi: 10.1371/journal.pone.0003355.

[17] Stokes, P. A. and Purdon, P. L. (2017) 'A study of problems encountered in Granger causality analysis from a neuroscience perspective', *Proceedings of the National Academy of Sciences of the United States of America*, 114(34), pp. E7063–E7072. doi: 10.1073/pnas.1704663114.

[18] Kim, H. J. (2011) 'Isolation and Culture of Neurons and Astrocytes from the Mouse Brain Cortex', 0, pp. 63–75. doi: 10.1039/9781849733014.

[19] Shadlen MN, Newsome WT (1994) 'Noise, neural codes and cortical organization.', *Curr Opin Neurobiol.* Aug;4(4), pp. 569-79. doi: 10.1016/0959-4388(94)90059.

[20] Wagenaar, D. A. *et al.* (2009) 'Controlling Bursting in Cortical Cultures with Closed-Loop Multi- Electrode Stimulation', *Technology*, 25(3), pp. 680–688. doi: 10.1523/JNEUROSCI.4209-04.2005.Controlling.

[21] Lloyd, E. K., Bondy, J. A. and Murty, U. S. R. (1978) 'Graph Theory with Applications', *The Mathematical Gazette*, 62(419), p. 63. doi: 10.2307/3617646.

[22] Bredon, G. E. (1993) *Topology and Geometery*. Available at: http://library1.nida.ac.th/termpaper6/sd/2554/19755.pdf.

[23] West, D. B. (2009) 'Introduction to graph theory', *Introduction to Graph Theory*, pp. 1–144.

[24] Sporns, O. (2018) 'Graph theory methods: Applications in brain networks', *Dialogues in Clinical Neuroscience*, 20(2), pp. 111–120. doi: 10.31887/DCNS.2018.20.2/OSPORNS.

[25] Madhavan, R., Chao, Z. C. and Potter, S. M. (2007) 'Plasticity of recurring spatiotemporal activity patterns in cortical networks.', *Physical biology*, 4(3), pp. 181–93. doi: 10.1088/1478-3975/4/3/005.

[26] Wagenaar, D. A., Pine, J. and Potter, S. M. (2006) 'An extremely rich repertoire of bursting patterns during the development of cortical cultures', *BMC Neuroscience*, 7, pp. 1–18. doi: 10.1186/1471-2202-7-11.

[27] Zhu, M. J. *et al.* (2020) 'Identifying the pulsed neuron networks' structures by a nonlinear Granger causality method', *BMC Neuroscience*. BioMed Central, 21(1), pp. 1–9. doi: 10.1186/s12868-020-0555-z.

[28] Frega, M. *et al.* (2012) 'Cortical cultures coupled to Micro-Electrode Arrays: A novel approach to perform in vitro excitotoxicity testing', *Neurotoxicology and Teratology*. Elsevier Inc., 34(1), pp. 116–127. doi: 10.1016/j.ntt.2011.08.001.

[29] Wagenaar, D. A., Pine, J. and Potter, S. M. (2004) 'Effective parameters for stimulation of dissociated cultures using multi-electrode arrays', *Journal of Neuroscience Methods*, 138(1–2), pp. 27–37. doi: 10.1016/j.jneumeth.2004.03.005.

[30] Odawara, A. *et al.* (2016) 'Physiological maturation and drug responses of human induced pluripotent stem cell-derived cortical neuronal networks in long-term culture', *Scientific Reports*. Nature Publishing Group, 6(April), pp. 1–14. doi: 10.1038/srep26181.

[31] Plenz, D. *et al.* (2011) 'Multi-electrode Array Recordings of Neuronal Avalanches in Organotypic Cultures', *Journal of Visualized Experiments*, (54), pp. 2–7. doi: 10.3791/2949.

[32] Gracia-Tabuenca, Z. *et al.* (2019) 'Topological Data Analysis reveals robust alterations in the whole-brain and frontal lobe functional connectomes in Attention-Deficit/Hyperactivity Disorder', *bioRxiv*, 7(June). doi: 10.1101/751008.

[33] Setia, H. and Muotri, A. R. (2019) 'Brain organoids as a model system for human neurodevelopment and disease', *Seminars in Cell and Developmental Biology*. Elsevier, 95(August 2018), pp. 93–97. doi: 10.1016/j.semcdb.2019.03.002.